ADVANCED FUNCTIONAL MATERIALS

Supporting Information

for *Adv. Funct. Mater.,* DOI: 10.1002/adfm.202200973

Manipulating Picosecond Photoresponse in van der Waals Heterostructure Photodetectors

Zhouxiaosong Zeng, Cuihuan Ge, Kai Braun, Martin Eberle, Yufan Wang, Biyuan Zheng, Chenguang Zhu, Xingxia Sun, Lanyu Huang, Ziyu Luo, Ying Chen, Huigao Duan, Shuangyin Wang, Dong Li, Fei Gao, Anlian Pan, and Xiao Wang**

Supporting Information

Manipulating picosecond photoresponse in van der Waals heterostructure photodetectors

Zhouxiaosong Zeng , Cuihuan Ge , Kai Braun, Martin Eberle, Yufan Wang, Biyuan Zheng, Chenguang Zhu, Xingxia Sun, Lanyu Huang, Ziyu Luo, Ying Chen, Huigao Duan, Shuangyin Wang, Dong Li, Fei Gao, Anlian Pan, Xiao Wang**

Prof. X. Wang, Dr. Z. Zeng, C. Ge, Y, Wang, L, Huang
School of Physics and Electronics, Hunan University, Changsha 410082, China
Dr. K. Braun, M. Eberle
Institute of Physical and Theoretical Chemistry and LISA+, University of Tübingen, Auf der Morgenstelle 18, 72076, Tübingen, Germany
Prof. A. Pan, Dr. B. Zheng, C. Zhu, X. Sun, Z. Luo, Y, Chen, Prof. D. Li
Key Laboratory for Micro-Nano Physics and Technology of Hunan Province, College of Materials Science and Engineering, Hunan University, Changsha, 410082, China
Prof. H. Duan
State Key Laboratory of Advanced Design and Manufacturing for Vehicle Body College of Mechanical and Vehicle Engineering, Hunan University, Changsha, 410082, China
Prof. S. Wang
State Key Laboratory of Chem/Bio-Sensing and Chemometrics, College of Chemistry and Chemical Engineering, Hunan University, Changsha, 410082, China
Prof. F. Gao
Department of Nuclear Engineering and Radiological Sciences, University of Michigan, Ann Arbor, Michigan, 48109, United States
E-mail: anlian.pan@hnu.edu.cn; xiao_wang@hnu.edu.cn

Contents:

Section 1. Electric transport properties of fabricated devices

Transfer characteristics of monolayer MoS_2, 25 nm WSe_2, and monolayer WSe_2 devices were measured to evaluate material transport properties, as shown in Figure S1a-c. The monolayer MoS_2 device exhibits an on/off ratio of approximately 10^6 with a threshold voltage of -60 V, manifesting its highly electron-doped property. Meanwhile, with the decrease in WSe_2 thickness, a transition from ambipolar to preferential-n-type transfer characteristics can be found in 25 nm WSe_2 and monolayer WSe_2 devices, respectively, which ensures our construction of p-n and n-n heterostructure devices. Based on the transconductance, we calculated the carrier mobility of these fabricated devices using the equation:

$$\mu_0 = [dI_{ds}/dV_{bg}] \times [L/WC_iV_{ds}],$$

where L/W is the ratio between the channel length and width, and C_i is the capacitance between the back gate per unit area (in our case $C_i = 1.15\times 10^{-8}$ F cm^{-2} for 300 nm thick SiO_2). The results reveal values around 11.5 cm^{2}V^{-1}s^{-1} for monolayer MoS_2 (Figure S1d), 25.3 cm^{2}V^{-1}s^{-1} for 23 nm WSe_2 (Figure S1e), and the 3.1 cm^{2}V^{-1}s^{-1} for monolayer WSe_2 (Figure S1f).

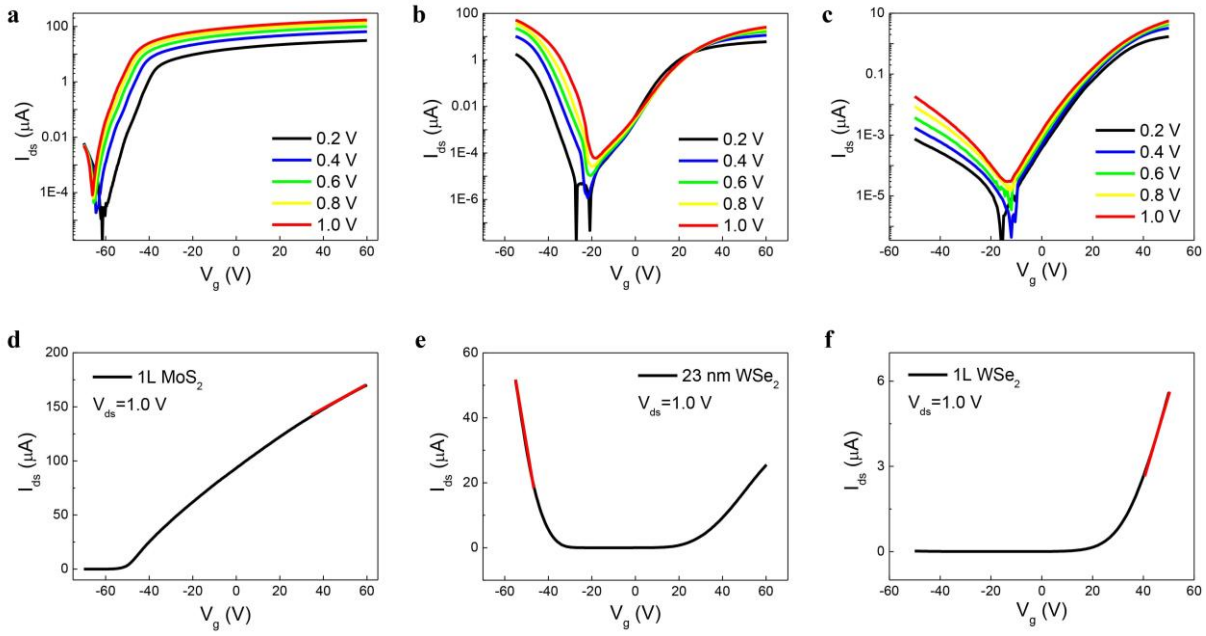

Figure S1. a-c) Transfer characteristic curves of monolayer MoS_2, 25 nm WSe_2, and monolayer WSe_2 in semi-log scale at drain voltages from 0.2 V to 1 V. d-f) Transfer

characteristic curves of monolayer MoS_2, 25 nm WSe_2, and monolayer WSe_2 in linear scale at 1 V drain voltage.

Section 2. Optical measurements of 1L MoS_2/1L WSe_2

To ensure our fabricated heterostructure devices have good electric transport and photoresponse properties, Raman, photoluminescence (PL), and time-resolved photoluminescence (TRPL) measurements were performed to examine the material interlayer coupling. In Raman spectra of 1L MoS_2/1L WSe_2 device (Figure S2d-f), typical signatures of WSe_2 peak (2*LA*(*M*) at 260 cm^{-1}) and MoS_2 peaks (A_{1g} at 405 cm^{-1} and E_{2g} at 384 cm^{-1})[1,2] were observed, determining the construction of the desired heterostructure. In PL measurements, the emission of MoS_2 and WSe_2 peaks from the overlapped region in heterostructure was strongly quenched, and a prominent red-shift of the WSe_2 peak from 750 nm to 773 nm could be found (Figure S2a). Meanwhile, in TRPL measurements, compared with the pure material, the PL decays of both MoS_2 and WSe_2 in heterostructure were accelerated and their carrier lifetimes were reduced (Figure S2b and S2c), indicating the efficient carrier transfer in type-II heterostructure and the high quality of our fabricated device.

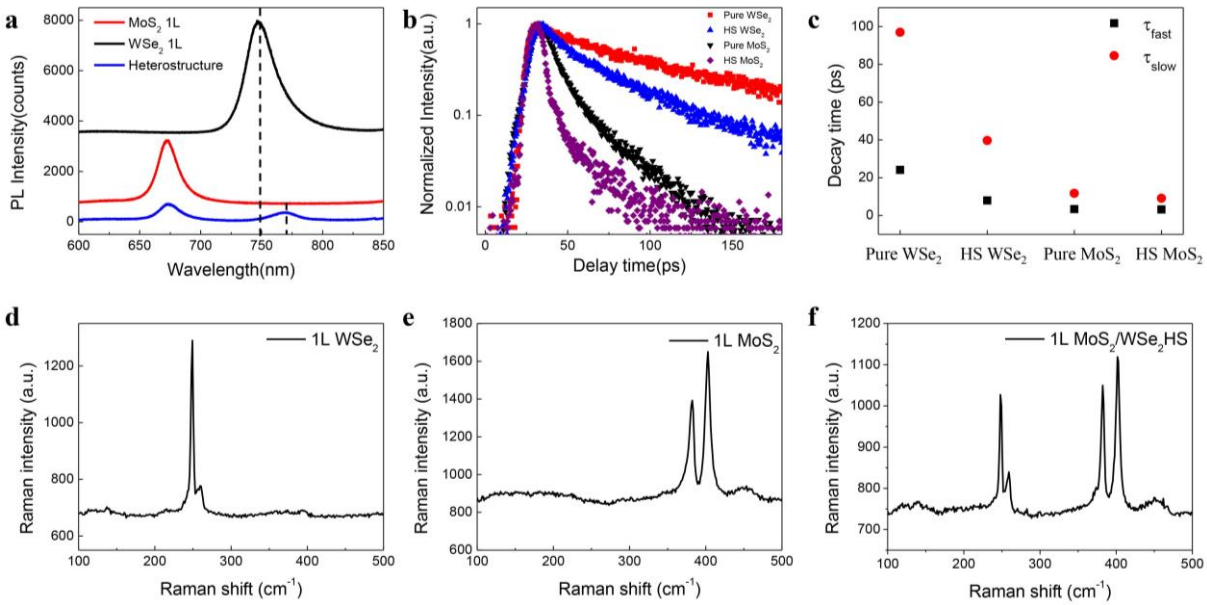

Figure S2. a) PL spectra recorded from heterostructure at different regions. b) Time-resolved photoluminescence (TRPL) decay in heterostructure at different regions. c) Extracted lifetimes for different materials from (b). d-f) Raman spectra in heterostructure at different regions.

Section 3. Scanning photocurrent Microscope (SPCM) of fabricated devices

SPCM measurements of 1L MoS_2/1L WSe_2 (Figure S3b) and 1L MoS_2/4 nm WSe_2 (Figure S3d) devices were also conducted by the excitation of 488 nm continuous wave (CW) laser to investigate the pure photovoltaic (PV) response. Compared with the 780 nm laser excitation, the 488 nm laser excited SPCM images exhibit that the photocurrent maximum exactly appears at the overlapped region between two electrodes with the reduced diffusion length, which is explained as the decreased photothermoelectric (PTE) effect contribution and the enhanced optical resolution of the excitation laser. Meanwhile, we attribute the larger photocurrent intensity by the 488 nm laser excitation compared with that by the 780 nm laser excitation studied in the main text Figure 3 to the total photo-absorption of both MoS_2 and WSe_2 layers.

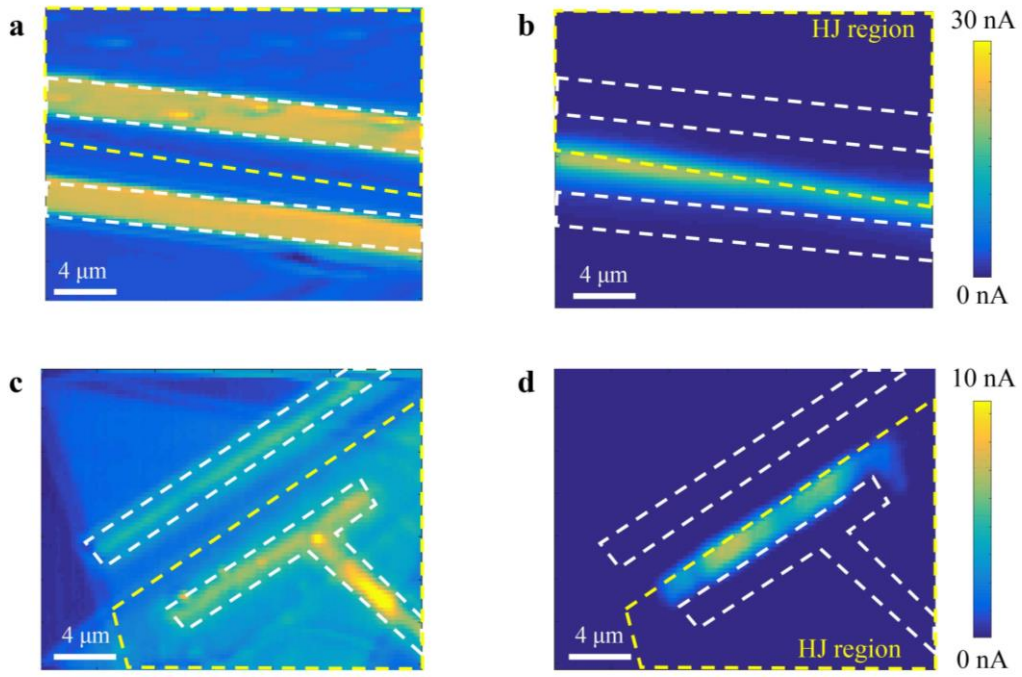

Figure S3. a) and c) Reflective optical image of 1L MoS_2/1L WSe_2 and 1L MoS_2/ 4 nm WSe_2 devices corresponding to that studied in the main text Figure 3. b) and d) Corresponding SPCM mappings with the excitation of 488 nm CW laser.

Section 4. Pump power induced Time-resolved photocurrent (TRPC) of 1L MoS_2/1L WSe_2 devices

For the 1L MoS_2/1L WSe_2 device studied in the main text, we fitted its photocurrent decays at different pump powers (Figure S4a-f) using the equation:

$$\frac{PC(\Delta t)}{PC(\Delta t \rightarrow \infty)} = 1 - A\exp(-\frac{\Delta t}{\tau_1}) - B\exp(-\frac{\Delta t}{\tau_2}),$$

and the results yield that all the decay curves have the response time τ_{fast} of approximate 5 ps (50% to 75% of weight) with a slight increase at the small excitation pump powers. Meanwhile, a slow component τ_{slow} of approximate 30 ps (25% to 50% of weight) was also observed in almost every decay curve, which could be derived from the charge carrier transfer in heterostructure similar to our previous report.[3]

In the main text Figure 4a and 4b, pump power-dependent TRPC in 1L MoS_2/1L WSe_2 heterostructure device exhibits a phenomenon that with the increase in pump power, the TPRC peak at zero pump-probe delay gradually increased while the photocurrent background was suppressed. Besides this typical phenomenon, other two different situations can also occur. In the second 1L MoS_2/1L WSe_2 heterostructure device (Figure S5a), with the existence of pump power, though the photocurrent background was suppressed similarly to the phenonmenon in the main text, an enhanced TRPC peak signal at zero pump-probe delay over the photocurrent without pump power was obtained (Figure S5b). Further, in the third 1L MoS_2/1L WSe_2 heterostructure device (Figure S6a), with the existence of pump power, both photocurrent background and the TRPC peak were enhanced (Figure S6b). For the above phenomena, we explain them as the different degrees of the photocurrent offset between PV and PTE effects without pump beam and the different degrees of the suppression of PV and PTE effects inhibited from pump beam. Therefore, with the increase in pump power, the net photocurrent is different. Meanwhile, in these two distinct situations, a similar photocurrent response compared to that of the device studied in the main text can be obtained.

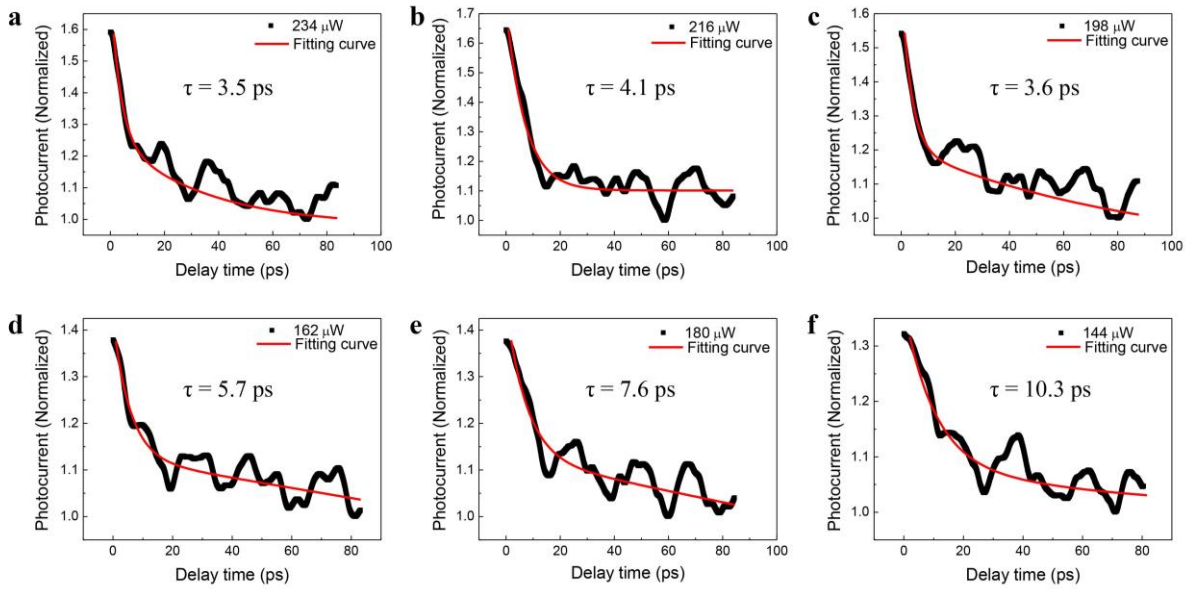

Figure S4. Normalized TRPC in 1L MoS_2/1L WS_2 heterostructure device at different pump powers. a) 234 μW, b) 216 μW, c) 198μW, d) 162 μW, e) 180 μW, f) 144 μW.

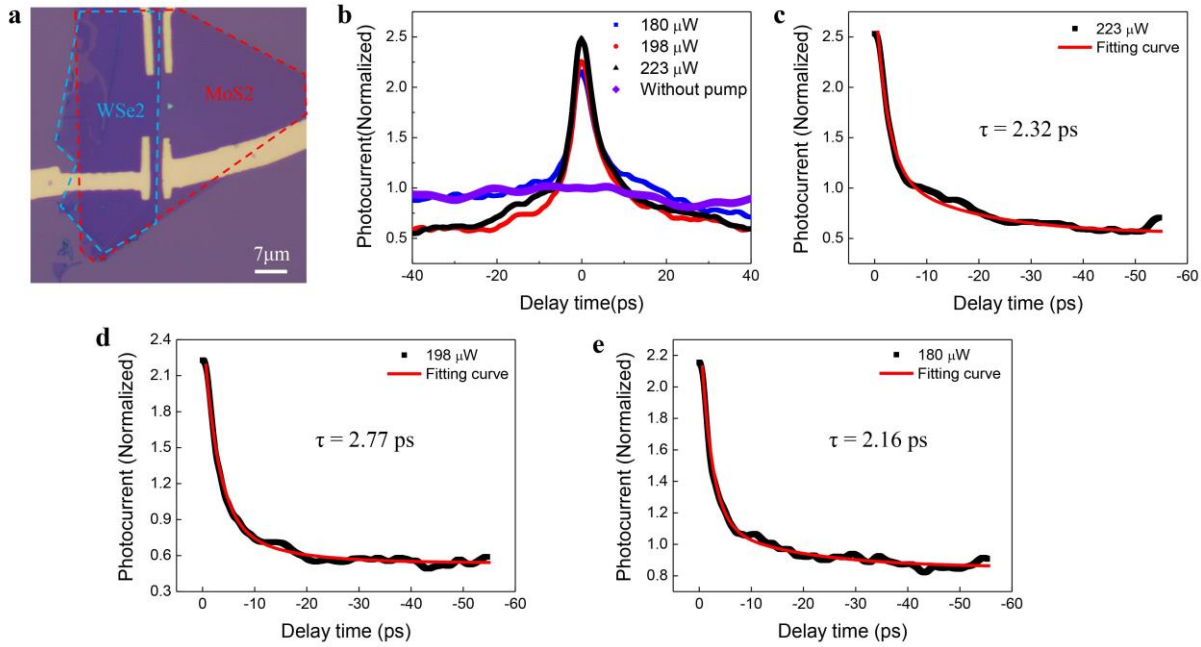

Figure S5. a) Optical images of the 1L MoS_2/1L WS_2 heterostructure device. b) TRPC measurements at different pump powers. c-e) Normalized TRPC at pump powers from 223 μW to 180 μW.

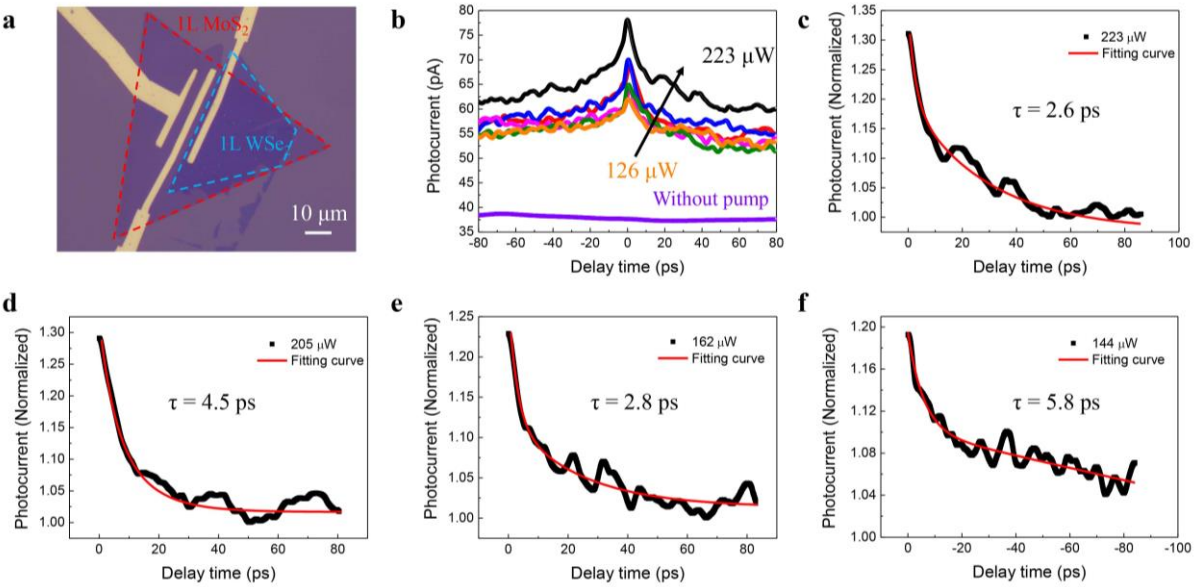

Figure S6. a) Optical images of the 1L MoS_2/1L WS_2 heterostructure device. b) TRPC measurements at different pump powers. e-f) Normalized TRPC at pump powers from 223 μW to 144 μW.

Section 5. Photocurrent polarization in pure monolayer MoS_2 and 1L MoS_2/1L WSe_2 heterostructure devices

To investigate the photocurrent response difference between PV and PTE effects, We performed the linearly polarized photocurrent measurements in pure monolayer MoS_2 and 1L MoS_2/1L WSe_2 heterostructure devices by the rotation of excitation laser using a half-wave plate (Figure S7a). In the pure monolayer MoS_2 device, the pure PV or PTE photocurrent response can be obtained by the excitation of 488 nm CW laser or 780 nm pulsed laser, respectively. Under the excitation of 488 nm laser, the monolayer MoS_2 device exhibits an anisotropy ratio of 1.1 (Figure S7b), indicating a nonpolar photoresponse of intrinsic MoS_2. While with the excitation of 780 nm laser, an anisotropy ratio of 4.25 with the maximum photocurrent parallel to the electrode can be found (Figure S7c), which is similar to the results in previous work reflecting a high-polarized PTE current response by the plasmonic effect from the electrodes.[4] In the heterostructure device, the PV response from the excitation of 488 nm laser is similar to the situation in pure monolayer MoS_2, showing almost unchanged photocurrent intensity with the different excitation azimuth angles (Figure S7d). While a maximum anisotropy ratio of 1.63 can be obtained at the excitation of 780 nm laser with and without pump power, which could be derived from the interaction between the PV and PTE effects in the heterostructure. Further, we normalized and compared the TRPC decays in 1L MoS_2/1L WSe_2 heterostructure with the excitation polarization parallel and perpendicular to the electrode (black and red curves in Figure S7f), and the results yield a similar fast photocurrent decay component of approximate 4 ps.

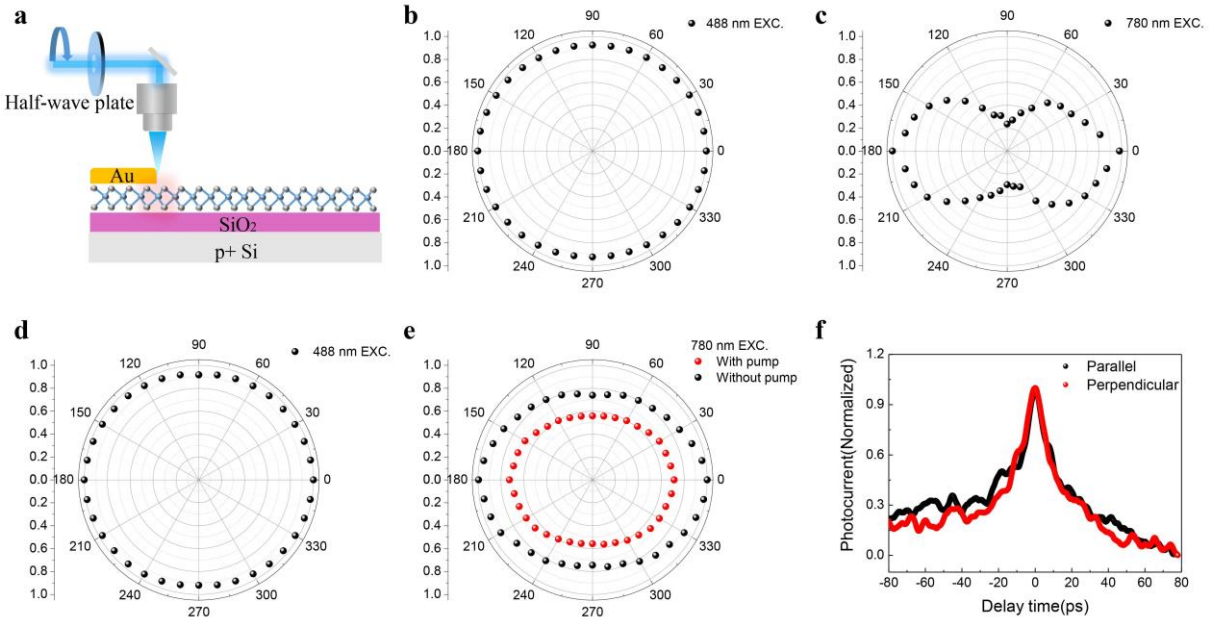

Figure S7. a) Schematic illustration of the linearly polarized photocurrent measurements by the rotation of a half-wave plate. b) and c) Polarization-dependent photocurrents in pure MoS_2 device with the excitation of 488 nm and 780 nm. d) and e) Polarization-dependent photocurrent in 1L MoS_2/1L WSe_2 heterostructure device with the excitation of 488 nm and 780 nm. f) Normalized TRPC measurement in 1L MoS_2/1L WSe_2 heterostructure device under the parallel and perpendicular excitation configurations.

Section 6. TRPC of 1L MoS_2/1L WSe_2 heterostructure device with different drain voltages

We normalized TRPC signals in 1L MoS_2/1L WSe_2 heterostructure device with different drain voltages. The results yield that there is an almost unchanged TRPC peak or dip proportion to the photocurrent background (Figure S8a-e). Besides, we compared TRPC signals at V_{ds} = 0 V and V_{ds} = 1 V, and the obtained faster response with the external bias indicates that the ultrafast response in 1L MoS_2/1L WSe_2 heterostructure device can be further enhanced by decreasing the carrier drift time (Figure S8f).

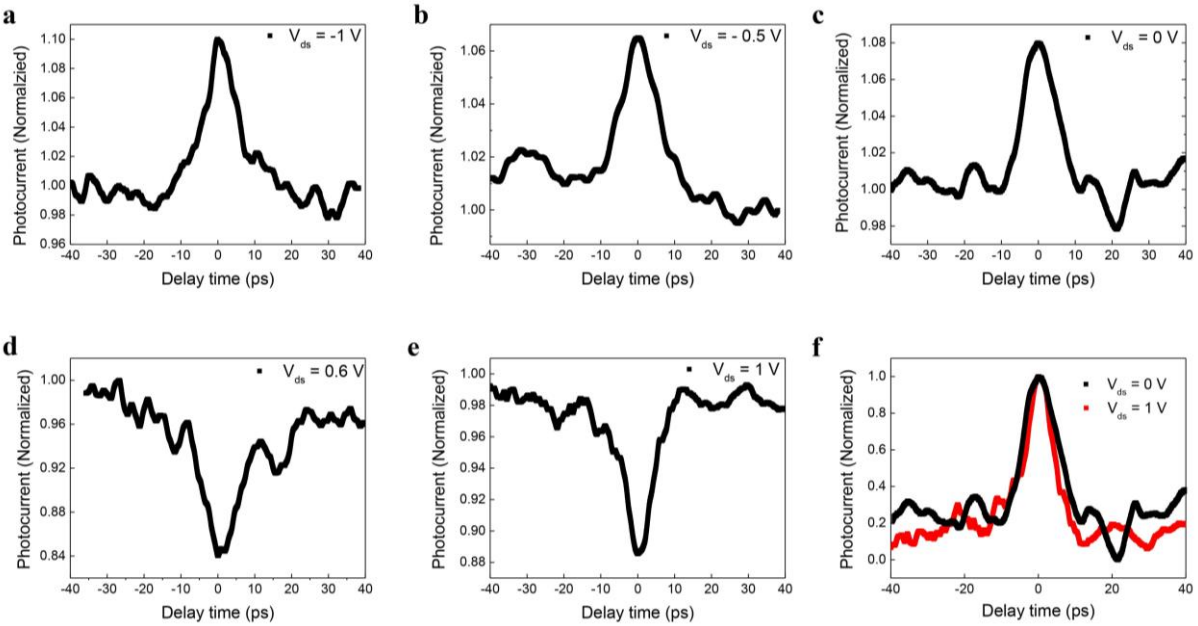

Figure S8. Normalized TRPC of 1L MoS_2/1L WSe_2 heterostructure device with different drain voltages. a) V_{ds} = -1 V, b) V_{ds} = -0.5 V, c) V_{ds} = 0 V, d) V_{ds} = 0.6 V, e) V_{ds} = 1 V. f) Comparison of the TRPC at V_{ds} = 0 V and V_{ds} = 1 V, showing the device response time can be further reduced by the external bias.

Section 7. Photocurrent response on pure monolayer MoS_2 device

We performed photocurrent response measurements in a pure monolayer MoS_2 device (Figure S9a) with the excitation of a 780 nm pulse laser. Because the energy of excitation laser 1.59 eV is lower than the bandgap of monolayer MoS_2 approximately 1.85 eV, the photocurrent response is considered as the pure PTE effect. In SPCM images, a PTE current can be obtained at the junctions between the MoS_2 flake and the electrodes (Figure S9f) similar to the situation in the PV effect (Figure S9e), but it is attributed to the large Seebeck coefficient difference between semiconductors and metals. With the increase in individual probe beam power, a PTE current saturation can be also observed (Figure S9b), but there is no obvious photocurrent recovery with the increase in pump-probe delay (Figure S9c). Hence we consider that the PTE current is invariant in our measurement time window and the hot carrier's relaxation time could be at least hundreds of nanoseconds in monolayer MoS_2.

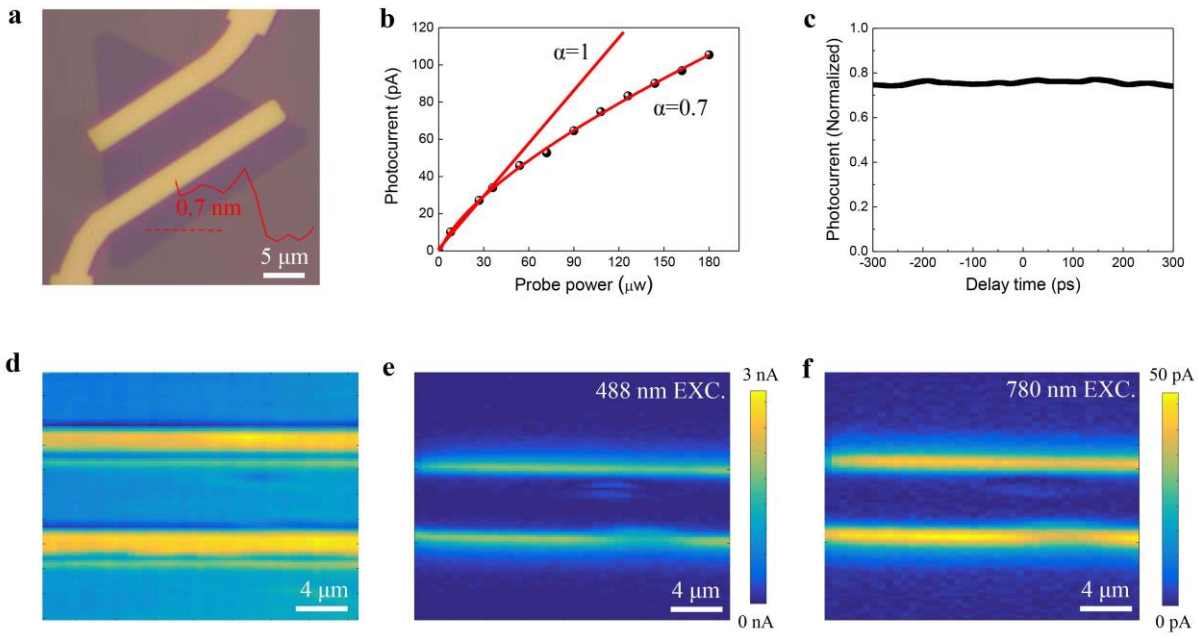

Figure S9. a) Optical image of monolayer MoS_2 device. The inset atomic layer force (AFM) line scan indicates its thickness. b) PTE current response as the function of 780 nm probe power without the pump. c) TRPC measurement shows almost unchanged carrier dynamics by the PTE effect. d) Reflective image of monolayer MoS_2 device. The yellow rectangles indicate the position of the electrodes. e) and f) SPCM images of monolayer MoS_2 device with the excitation of 488 nm CW laser and 780 nm pulsed laser.

Section 8. Discussion on the performance of ultrafast two-dimensional (2D) material photodetectors

In this section, we make a discussion about the performance of ultrafast 2D material photodetectors. Though the conventional PV and PTE devices have been investigated, the studies concerning their interactions in one device remain unexplored owning to the sophisticated device design. Our studies using the TRPC technique in combination of SPCM measurements focus on the PV and PTE effects induced ultrafast photogenerated carrier dynamics, and observe a distinct TRPC peak in n-n junction, indicating the opposite polarity between PV and PTE effects. These results could provide a guideline to some specific self-powered photodetectors that need to improve their efficiency or find their higher conversion via separating different photocurrent contribution mechanisms.

Here we make an estimation about the quantitative photocurrent contribution ratio of PTE and PV effects according to some published literature. We first determine the Seebeck coefficient for pure monolayer MoS_2 and pure monolayer WSe_2 under $V_g = 0$ V and $V_{ds} = 0$ V based on the formula $V_T = (S_1\text{-}S_2)\ \Delta T$. In the illumination of 780 nm laser with 50 μW power, the measured photothermoelectric voltages in pure monolayer MoS_2 and pure monolayer WSe_2 device are approximate 80 μV and 5 mV, respectively. If we take the junction temperature increment (at the electrode) ΔT as 0.13 K for pure monolayer MoS_2 and pure monolayer WSe_2 device similar to the previous work[5] and neglect the Seebeck coefficient of the metal electrode because its value is far smaller than that of semiconductors,[6] the calculated Seebeck coefficient for pure monolayer MoS_2 and pure monolayer WSe_2 under 0 V gate voltage are approximate 0.62 mV/K and 38 mV/K, respectively. Meanwhile, if we treat the junction temperature increment ΔT in a MoS_2/1L WSe_2 heterostructure as 1 mK, then the generated V_T in a MoS_2/1L WSe_2 heterostructure is 37.38 μV and corresponds to 30 pA. In this case, the photocurrent generation ratio between PTE and PV is approximate 1:3 in the

SPCM image in Figure 3b. But it is worthwhile to emphasize that this value could be totally different in TRPC measurements because of the different suppression by the pump laser between PTE and PV effects.

Besides, two-dimension (2D) materials hold great advantages with their atomically thin thickness, thus the transit time τ_r of 2D vertical devices could be extremely shortened, which demonstrates the potential in ultrafast optoelectronic applications. A recent work[7] demonstrates that the vertical graphene/$MoTe_2$ near-infrared photoconductive photodetectors with the integration of Si waveguide possess high-responsivity and high response speed, because the collection path of photo-generated carriers perpendicular to the light propagation direction along the waveguide avoids the trade-off between transit time and light absorption. Hence, the design of self-powered p-n and n-n junctions could be improved with the same design and are expected to realize the nearly intrinsic ultrafast response speed without an external bias.

References

[1] W. Zhao, Z. Ghorannevis, K. K. Amara, J. R. Pang, M. Toh, X. Zhang, C. Kloc, P. H. Tan, G. Eda, *Nanoscale* **2013**, *5*, 9677.

[2] F. Li, Y. X. Feng, Z. W. Li, C. Ma, J. Y. Qu, X. P. Wu, D. Li, X. H. Zhang, T. F. Yang, Y. Q. He, H. L. Li, X. L. Hu, P. Fan, Y. Chen, B. Y. Zheng, X. L. Zhu, X. Wang, X. F. Duan, A. L. Pan, *Adv. Mater.* **2019**, *31*, 1901351.

[3] Z. Zeng, K. Braun, C. Ge, M. Eberle, C. Zhu, X. Sun, X. Yang, J. Yi, D. Liang, Y. Wang, L. Huang, Z. Luo, D. Li, A. Pan, X. Wang, *(Preprint) Fundam. Res.*, https://doi.org/10.1016/j.fmre.2021.09.018, 9 **2021**.

[4] T. Hong, B. Chamlagain, S. R. Hu, S. M. Weiss, Z. X. Zhou, Y. Q. Xu, *ACS Nano* **2015**, *9*, 5357.

[5] M. Buscema, M. Barkelid, V. Zwiller, H. S. J. van der Zant, G. A. Steele, A. Castellanos-Gomez, *Nano Lett.* **2013**, *13*, 358.

[6] J. Wu, H. Schmidt, K. K. Amara, X. F. Xu, G. Eda, B. Ozyilmaz, *Nano Lett.* **2014**, *14*, 2730.

[7] N. Flory, P. Ma, Y. Salamin, A. Emboras, T. Taniguchi, K. Watanabe, J. Leuthold, L. Novotny, *Nat. Nanotechnol.* **2020**, *15*, 118.